J. of Supercritical Fluids 68 (2012) 1–12

Contents lists available at SciVerse ScienceDirect

The Journal of Supercritical Fluids

journal homepage: www.elsevier.com/locate/supflu

One-dimensional model for heat transfer to a supercritical water flow in a tube

Joost L.H.P. Sallevelt[a,*], Jan A.M. Withag[a], Eddy A. Bramer[a], Derk W.F. Brilman[b], Gerrit Brem[a]

[a] University of Twente, Department of Thermal Engineering, Faculty of Engineering Technology, 7500 AE Enschede, The Netherlands
[b] University of Twente, Thermo-Chemical Conversion of Biomass (TCCB), Faculty of Science and Technology, 7500 AE Enschede, The Netherlands

ARTICLE INFO

Article history:
Received 12 January 2012
Received in revised form 5 April 2012
Accepted 6 April 2012

Keywords:
Supercritical water
Heat transfer
1D model
Nusselt correlation
System model

ABSTRACT

Heat transfer in water at supercritical pressures has been investigated numerically using a one-dimensional modeling approach. A 1D plug flow model has been developed in order to make fast predictions of the bulk-fluid temperature in a tubular flow. The chosen geometry is a vertical tube with an inner diameter of 10 mm and a heated length of 4.0 m.

The simulations concern a heated upward flow with an imposed wall temperature profile. Viscous effects, internal conduction and enthalpy changes due to a pressure gradient have been neglected after evaluation of the governing equations in dimensionless form. The resulting set of equations is closed using Nusselt correlations found in literature and solved using an explicit Euler scheme to simulate heat transfer in a supercritical water flow.

The results for three different cases show that the model is able to accurately predict the bulk temperature based on heat transfer rates provided by a suitable Nusselt correlation. However, there is also reason to assume that these correlations are very specific for the flow conditions, since boiling effects occurring at certain conditions can highly influence the heat transfer rate. As a consequence, the model may be unable to describe supercritical heat transfer over a broad range of configurations when only using one correlation. The agreement of these results with the two-dimensional simulations will be investigated in a separate article.

The description of the model is preceded by a mathematical description of supercritical water flows and by an overview of the supercritical heat transfer phenomena as observed in earlier studies.

1. Theory of supercritical water flows

This section is a general description of a water flow at supercritical conditions. Section 1.1 deals with the equations that describe the flow field and heat transfer. Next, Section 1.2 elaborates on the formulation that is used to calculate the relevant thermodynamic and transport properties of water. Section 1.3 gives a more qualitative description of the characteristics of the flow on basis of information found in the literature.

1.1. Governing equations

The equations that describe the flow follow from the laws of conservation of mass, momentum, energy and species [1]. Starting with mass, the conservation principle is mathematically described by:

$$\frac{\partial \rho}{\partial t} + \vec{\nabla} \cdot (\rho \vec{u}) = 0 \tag{1}$$

where ρ is the mass density and $\vec{u} = (u, v, w)^T$ the velocity of the mixture. Conservation of momentum can be stated as the following vector equation, also referred to as the Navier–Stokes equations:

$$\frac{\partial (\rho \vec{u})}{\partial t} + \vec{\nabla} \cdot (\rho \vec{u}\vec{u}) = -\vec{\nabla} p - \vec{\nabla} \cdot \vec{\vec{\tau}} + \rho \vec{f} \tag{2}$$

where $\vec{\vec{\tau}}$ is the viscous stress tensor and $\vec{f}$ is the volumetric force vector. For a Newtonian fluid like water, the viscous stresses are described by Newton's law of viscosity, which reads in general form:

$$\vec{\vec{\tau}} = -\mu(\vec{\nabla}\vec{u} + (\vec{\nabla}\vec{u})^{\top}) + \left(\frac{2}{3}\mu - \kappa\right)(\vec{\nabla} \cdot \vec{u})\vec{\vec{\delta}} \tag{3}$$

where μ is the dynamic viscosity, κ is the dilatational viscosity and $\vec{\vec{\delta}}$ is the unity tensor.

Conservation of energy, in terms of total energy, is given by:

$$\frac{\partial (\rho E)}{\partial t} + \vec{\nabla} \cdot (\rho E \vec{u}) = \rho(\vec{f} \cdot \vec{u}) - \vec{\nabla} \cdot (p\vec{u}) - \vec{\nabla} \cdot (\vec{\vec{\tau}} \cdot \vec{u}) + \dot{Q} - \vec{\nabla} \cdot \vec{q} \tag{4}$$

Here $\dot{Q}$ is the volumetric heat source term and $\vec{q}$ is the heat flux vector. The heat flux vector is described by [2]:

$$\vec{q} = -k\vec{\nabla}T \tag{5}$$

* Corresponding author. Tel.: +31 53 489 4657; fax: +31 53 489 3663.
E-mail address: j.l.h.p.sallevelt@utwente.nl (J.L.H.P. Sallevelt).

0896-8446/$ – see front matter © 2012 Elsevier B.V. All rights reserved.
http://dx.doi.org/10.1016/j.supflu.2012.04.003

Dimensionless numbers

Bo	buoyancy parameter
Br	Brinkman number
Fr	Froude number
Gr	Grashof number based on temperature
Gr_q	Grashof number based on heat flux
Nu_{FT}	Nusselt number for forced convection according to the Dittus–Boelter equation
Nu	Nusselt number
Pe_D	Péclet number based on diameter
Pe	Péclet number based on length
Pr	Prandtl number
Ra	Rayleigh number
Re	Reynolds number
St	Stanton number

Greek symbols

α	thermal diffusivity [m^2 s]
β	volumetric expansion coefficient [1/K]
$\bar{\bar{\delta}}$	unity tensor
κ	dilatational viscosity [kg/(m s)]
μ	dynamic viscosity [kg/(m s)]
ν	kinematic viscosity [m^2 s]
ρ	mass density [kg/m^3]
$\bar{\bar{\tau}}$	viscous stress tensor [N/m^2]

Geometric definitions

D	tube diameter [m]
l	length of the heated tube section [m]
z	longitudinal coordinate [m]

Roman symbols

C_p	isobaric heat capacity [J/(kg K)]
$\overline{C}_p$	mean isobaric heat capacity [J/(kg K)]
E	total energy [J/kg]
e	internal energy [J/kg]
$\vec{f}$	volumetric force vector [m/s^2]
f	specific Helmholtz free energy [J/kg]
G	mass flux [kg/(m^2 s)]
g	gravitational acceleration [m/s^2]
g	specific Gibbs free energy [J/kg]
h	enthalpy [J/kg]
h	heat transfer coefficient [W/m^2 K]
k	thermal conductivity [W/m K]
L/D	length to diameter ratio
$\vec{n}_w$	outward-pointing normal unit vector
p	pressure [Pa]
$\dot{Q}$	volumetric heat source [W/m^3]
$\vec{q}$	wall heat flux vector [W/m^2]
q_{cr}	critical heat flux [W/m^2]
T	temperature [K or °C]
t	time [s]
T_{in}	tube inlet temperature [K or °C]
$\vec{u}$	velocity vector [m/s]

Subscripts

$(\ldots)_b$	evaluated at bulk conditions
$(\ldots)_{pc}$	evaluated at pseudo-critical conditions
$(\ldots)_w$	evaluated at wall conditions

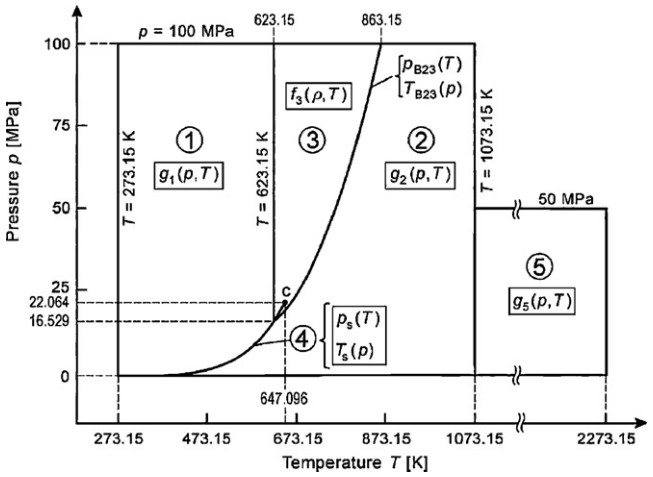

Fig. 1. The IAPWS-IF97 regions [5].
Reproduced with permission of Springer

The right-hand side of Eq. (5) represents thermal conduction, where k is the thermal conductivity of the fluid.

1.2. Thermophysical properties of supercritical water

The properties of water at different conditions are obtained using the Industrial Formulation 1997 [3] adopted by the International Association for the Properties of Water and Steam (IAPWS). The industrial formulation, abbreviated to IAPWS-IF97, was designed to closely approximate the values from the state of the art, high accuracy formulation IAPWS-95 [4] over a limited range of conditions.

In contrast to the single-equation IAPWS-95 standard, the IF97 formulation consists of a set of equations for five different regions [5] (see Fig. 1). For each region a basic equation was developed from which thermophysical properties such as specific volume, enthalpy and heat capacity can be derived. Regions 1, 2 and 5 are each covered by a fundamental equation for the specific Gibbs free energy $g(p, T)$, region 3 by a fundamental equation for the specific Helmholtz free energy $f(\rho, T)$. The advantage of using the Gibbs energy is that this equation has the pressure as an input quantity so that iterations are not necessary for given p, T values (W. Wagner, personal communication, May 28, 2011). However, this equation cannot be used for the entire thermodynamic surface since the pressure is the same at the bubble and dew line for given temperatures at the phase boundary. Therefore, different equations are needed for region 1 and 2. The reason why using the Helmholtz equation for region 3, which also contains the critical region, is that the Gibbs equation is unsuitable for representing the large changes in thermodynamic properties in this rather complex region. A Helmholtz equation is able to represent this region more accurately and with a shorter expression because the ρ, T surface is not as complicated as the p, T surface.

In addition, so-called backward equations were developed to efficiently calculate the state properties when using other input variables than needed for the basic equations. High numerical consistency across the region boundaries is achieved to ensure a smooth transition between the different sets of equations. Transport properties, in this study the thermal conductivity and viscosity, are calculated from supplementary equations provided by IAPWS.

The industrial standard offers easier numerical implementation and higher computational speed compared to the high accuracy standard, while the differences between the two formulations are small for most purposes. The estimated uncertainties in the industrial standard are the result of two contributions:

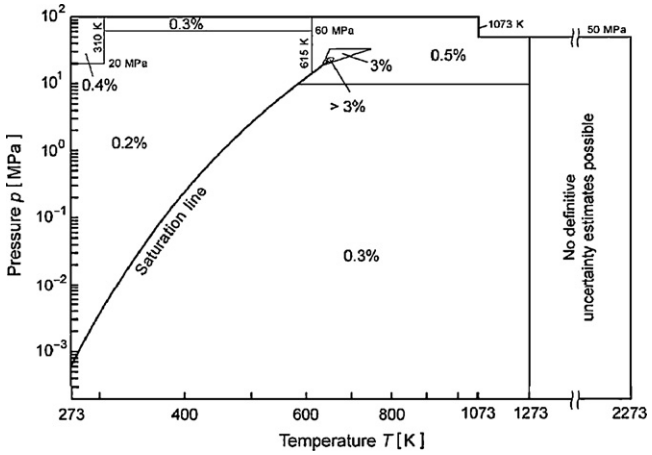

Fig. 2. Percentage uncertainties in specific isobaric heat capacity estimated for regions 1–3 and 5 [5].
Reproduced with permission of Springer.

uncertainties of the IAPWS-95 formulation, which was used for developing the IAPWS-IF97 basic equations, and deviations of IAPWS-IF97 from IAPWS-95. Considering the operating window of this study ($p = 241$ bar, $350 < T < 500\,^{\circ}$C), the combined uncertainty in specific volume is estimated to be less than 0.3%. Uncertainty percentages for the isobaric heat capacity are generally within 0.5%, but rise to 3% in the critical region and even more very near to the critical point (Fig. 2). Uncertainties in thermal conductivity and viscosity are given in terms of tolerances in tables with a uniform p–T grid. From these datapoints, it appears that k and μ are generally calculated with an accuracy well within 5% [6,7]. However, this percentage is exceeded in a small region around the critical point ($200 < p < 250$ bar, $350 < T < 400\,^{\circ}$C), where the estimated uncertainty is around 10%.

The accuracy of the IAPWS-IF97 formulation is considered sufficient for the simulations to be performed in this study. Detailed information on the mathematical background of the regions shown in Fig. 1 can be found in Wagner and Kretzschmar [5].

1.3. Characteristics of heat transfer to supercritical fluids

Prior to a discussion of the model and its results, it is useful to investigate the phenomena related to heat transfer to fluids at supercritical conditions. The main driving force for research activities in this field has been the development of nuclear power plants using SCW as the working fluid in order to improve thermal efficiency relative to existing nuclear plant designs [8]. Thanks to the work done on heat transfer to supercritical water in flow channels for new power plant designs, quite some information is available which can be built on. An overview of the most important and relevant phenomena, characteristics and expressions for heated fluid flows at supercritical pressures are given below.

In the literature dealing with heat transfer to tube flows at supercritical pressures, it is generally agreed that deviations from 'normal' heat transfer are observed [9]. Normal heat transfer here refers to single-phase heat transfer at sub-critical pressures described by the well-known Dittus–Boelter correlation [10]:

$$\mathrm{Nu} = 0.023\ \mathrm{Re}^{0.8}\ \mathrm{Pr}^{0.4} \tag{6}$$

where Nu, Re and Pr are the Nusselt, Reynolds and Prandtl numbers. Measurements show that deviations from normal heat transfer particularly occur when the wall temperature is higher than the pseudo-critical temperature, while the bulk temperature is below the pseudo-critical temperature ($T_w > T_{pc} > T_b$). In this situation, large thermo-physical property variations in the near-wall region

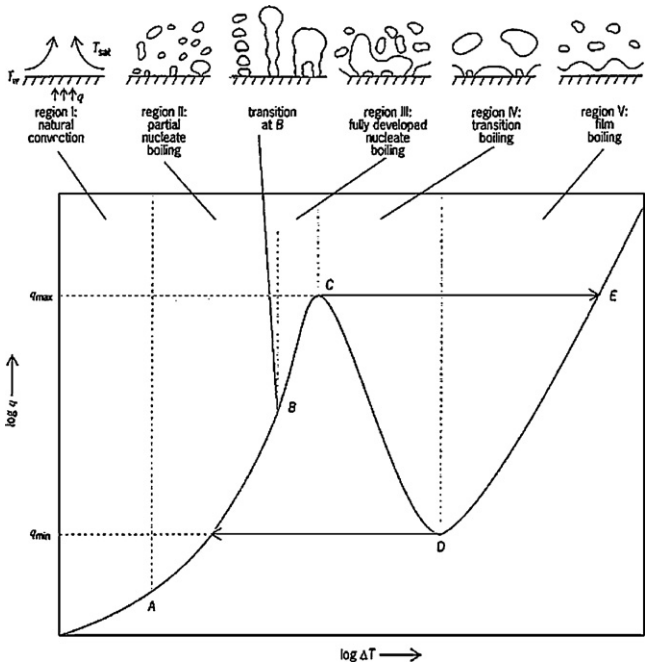

Fig. 3. Typical boiling curve, showing qualitatively the dependence of the wall heat flux, q, on the wall superheat, ΔT, defined as the difference between the wall temperature and the saturation temperature of the liquid [13].
Reproduced with permission of Annual Reviews.

can greatly affect heat transfer. Depending on the flow conditions, the variations in fluid properties can result in enhancement, impairment or deterioration of heat transfer. These observations may be explained by considering two boiling phenomena that possibly take place along the heated surface [11].

1.3.1. Boiling phenomena

One of these two boiling phenomena is pseudo-boiling [12]. Similar to nucleate boiling at subcritical pressures, low-density bubbles are formed at the hot wall where the fluid locally exceeds the pseudocritical temperature, while the bulk fluid is below the pseudocritical temperature. At some point the bubbles break loose from the heating surface and are carried into the bulk fluid, thereby transferring heat from the surface to the fluid stream quite effectively. Together with the agitation caused by the rising bubbles, this phenomenon results in enhancement of the heat transfer rate.

When the temperature is raised further, the heat transfer rate increases until the heat flux reaches a critical value. At this point, the rate of vaporization is such that dry patches occur over the heating surface, causing the rate of heat transfer to drop rapidly. At sufficiently high temperature differences, the entire surface is blanketed with a gas layer that prevents the liquid water from contacting the wall. Heat transfer then relies on the mechanism of conduction through the gaseous water film and radiation. This phenomenon is called pseudo-film boiling and is considered responsible for deterioration of the heat transfer rate. The effect of pseudo boiling and pseudo-film boiling on the heat flux is schematically shown in Fig. 3.

1.3.2. Critical heat flux

Studies on the heat flux at which pseudo-film boiling can occur, called the critical heat flux, has led to several correlations predicting the onset of heat transfer deterioration [14]. Large deviations are observed between the different correlations cited by Cheng et al. [14], but it is well agreed that the critical heat flux depends on the mass flux. Jackson and Hall [15] have suggested a correlation based on theoretical analysis of the effect of buoyancy on the shear stress.

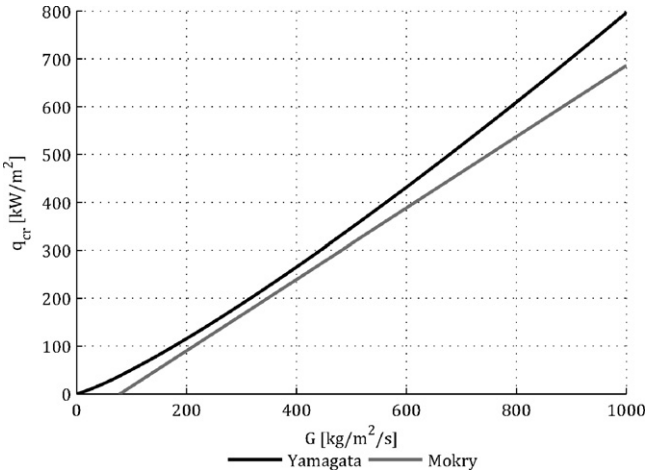

Fig. 4. Prediction of the critical heat flux as function of the mass flux using the correlations of Yamagata et al. [18] and Mokry et al. [8].

Two other theoretical models have been derived by Ogata and Sato [16] and Petuhkov and Kurganov [17]. These three semi-empirical correlations give much higher values for the critical heat flux than the empirical correlations. Possible reasons for the deviations can be found in the fact that Jackson and Hall noticed that the validity of their equation was not properly investigated, and that the other two correlations have been derived for fluids other than water.

The most relevant correlations for this study have been proposed by Yamagata et al. [18] and Mokry et al. [8] on basis of experimental data from supercritical water in a 10 mm tube. Yamagata et al. [18] derived a power law to correlate the critical heat flux q_{cr} kW/m^2 to the mass flux G kg/m^{2}s:

$$q_{cr} = 0.2 \cdot G^{1.2} \tag{7}$$

while Mokry et al. [8] found a linear relation between these parameters:

$$q_{cr} = -58.97 + 0.745 \cdot G \tag{8}$$

The critical heat flux as predicted by Eqs. (7) and (8) are plotted as a function of the mass flux in Fig. 4.

1.3.3. Buoyancy effects

Next to the boiling phenomena described above, literature points out that the accelerating low-density layer near the wall has considerable influence on the heat transfer rate as well [19–21]. Due to the buoyancy forces resulting from variations in density, the heat transfer mechanism can be a combination of forced and natural convection. In case the fluid is heated with upward flow or cooled down with downward flow, buoyancy effects aid forced convection since velocities due to natural and forced convection are in the same direction. This situation is called aiding flow, which shows very different heat transfer behavior from opposing flow, where the driving forces or natural and forced convection are in opposite direction.

The contribution of natural convection in relation to forced convective heat transfer depends on many conditions such as flow velocity, wall temperature and flow direction (aiding vs. opposing flow). Aicher and Martin [20] proposed the following criterium to compare the driving forces of the two types of convective heat transfer in turbulent flow in case of constant wall temperature:

$$\frac{\mathrm{Ra}^{0.333}}{\mathrm{Re}^{0.8}\mathrm{Pr}^{0.4}} \tag{9}$$

In this criterium, the Rayleigh number Ra characterizes the strength of the buoyancy forces. It is defined as the product of the Grashof number, which describes the relationship between buoyancy and viscosity, and the Prandtl number, which is the ratio of momentum diffusivity to thermal diffusivity:

$$\mathrm{Ra} = \mathrm{Gr} \cdot \mathrm{Pr} = \frac{g\beta(T_w - T_b)D^3}{\nu^2} \cdot \frac{\nu}{\alpha} = \frac{g\beta}{\nu\alpha}(T_w - T_b)D^3 \tag{10}$$

where g is the gravitational acceleration, β is the cubic expansion coefficient, ν is the kinematic viscosity and α is the thermal diffusivity. The Reynolds number Re in Eq. (9) compares the dynamic pressure to the shear stress acting on the fluid:

$$\mathrm{Re} = \frac{\rho u D}{\mu} \tag{11}$$

For aiding flow, natural convection is the dominant heat transfer mechanism if the parameter of Aicher and Martin exceeds 0.2. If less than 0.05, forced convection is dominating. The range in between indicates the mixed convection regime. The influence of buoyancy forces on heat transfer is schematically shown in Fig. 5. Here, the ratio between Nu and $\mathrm{Nu_{FT}}$ is plotted against the parameter of Eq. (9). $\mathrm{Nu_{FT}}$ is defined as the Nusselt number for 'normal' forced convection and is described by the Dittus–Boelter equation, Eq. (6).

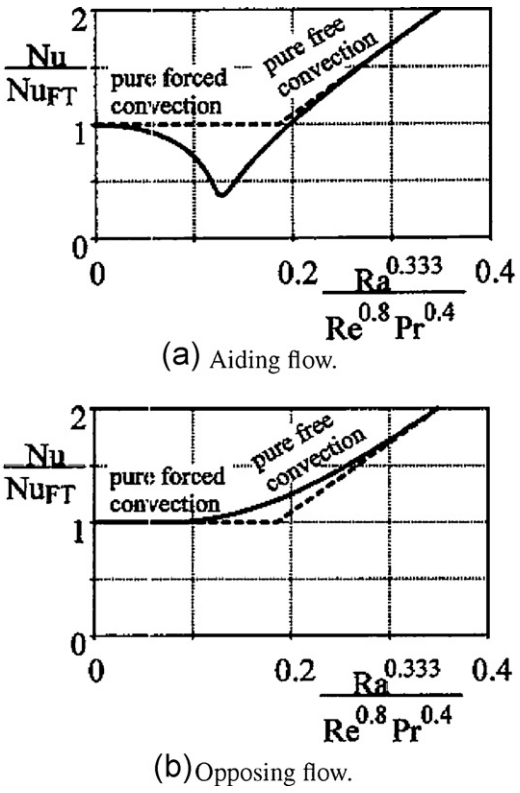

Fig. 5. Schematic view of the influence of buoyancy forces on heat transfer [20]. Reproduced with permission of Elsevier.

A similar criterium, defined as the buoyancy parameter Bo, was more recently presented for constant wall heat flux by Celata et al. [21], although originally developed by Jackson and Hall [15]:

$$Bo = 8 \times 10^4 \frac{\mathrm{Gr}_q}{\mathrm{Re}^{3.425}\mathrm{Pr}^{0.8}} \tag{12}$$

In this expression, fluid properties are evaluated at film temperature and the Grashof number, Gr_q, is based on the wall heat flux. Comparing Fig. 5 with the graph in Fig. 6, where the buoyancy parameter Bo is on the horizontal axis, the same behaviour of the normalized Nusselt number is observed. Celata et al. [21] showed

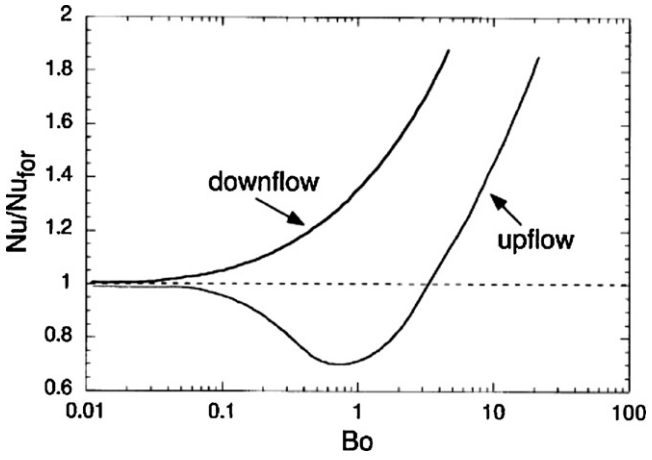

Fig. 6. Schematic view of heat transfer for aiding and opposing mixed convection [21].
Reproduced with permission of Elsevier.

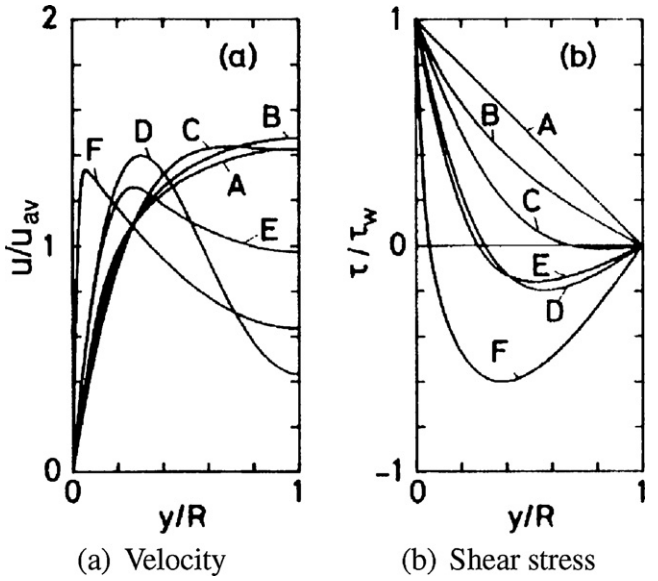

Fig. 7. Distributions at various Grashof numbers at a constant Re = 3000. (A) $Gr = 2.1 \times 10^3$, turbulent; (B) $Gr = 6.1 \times 10^4$, turbulent; (C) $Gr = 8.8 \times 10^4$, laminar; (D) $Gr = 2.7 \times 10^5$, laminar; (E) $Gr = 3.3 \times 10^5$, turbulent; (F) $Gr = 9.2 \times 10^6$, turbulent [22].
Reproduced with permission of Elsevier.

experimentally that the mixed convection region corresponds with values of Bo between 0.03 and 3.

The effect of buoyancy forces on the rate of heat transfer may be explained by considering the turbulence production between the viscous layer and the bulk flow [21,19]. In aiding flow, the fluid layer adjacent to the heated wall is subject to a buoyancy force which acts in the same flow direction. Therefore, buoyancy forces tend to reduce the shear stress in the layer, reducing turbulent diffusion of heat and thus causing deteriorated heat transfer. As the temperature of the fluid in the near-wall region increases further, density differences cause the low-density fluid to outrun the bulk flow. This restores the turbulence production and hence heat transfer, as is seen in Figs. 5 and 6. Typical examples of velocity profiles and shear stress distributions are shown in Fig. 7 [22]. With increasing buoyancy effects from profile A to profile F, shear stress is first decreased, but eventually reintroduced in opposite direction when the velocity of the low-density fluid is higher than the bulk velocity.

The different heat transfer regimes that can be discerned due to the phenomena discussed above have been illustrated by Licht et al. [19]. A schematic visualization of each regime and the effect on the heat transfer compared to normal heat transfer (with no property variations) is given in Fig. 8.

On basis of the information given in this section, the cases that have been considered in this study can be properly classified. By using terminology, expressions and criteria in agreement with existing literature on this topic, interpretation of the simulation results and comparisons with earlier work is facilitated. Three heated upflow cases are chosen for analysis, which only differ in mass flux. The first can be representative for industrial cooling purposes, the third case more likely describes a flow reactor which should provide enough residence time for the reacting species. The specifications of the three cases are listed in Table 1.

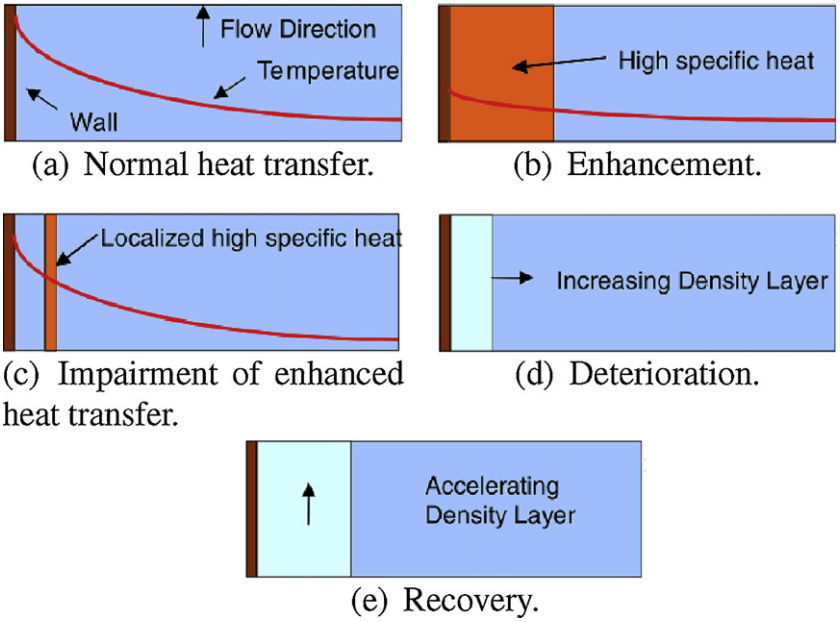

Fig. 8. Illustration of the different heat transfer regimes [19].
Reproduced with permission of Elsevier.

Table 1
Specification of the cases that are considered in this study.

Parameters	Symbol	Unit	Case 1	Case 2	Case 3
Inlet mass flux	G	kg/m^{2}s	1000	500	200
Pressure	p	bar	241	241	241
Inner diameter	D	mm	10	10	10
Length to diameter ratio	L/D	–	400	400	400
Inlet temperature	T_{in}	°C	350	350	350

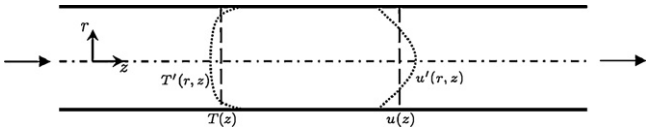

Fig. 9. Physical domain for the 1D model.

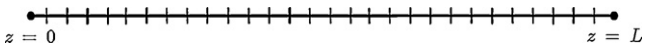

Fig. 10. Computational domain for the 1D model.

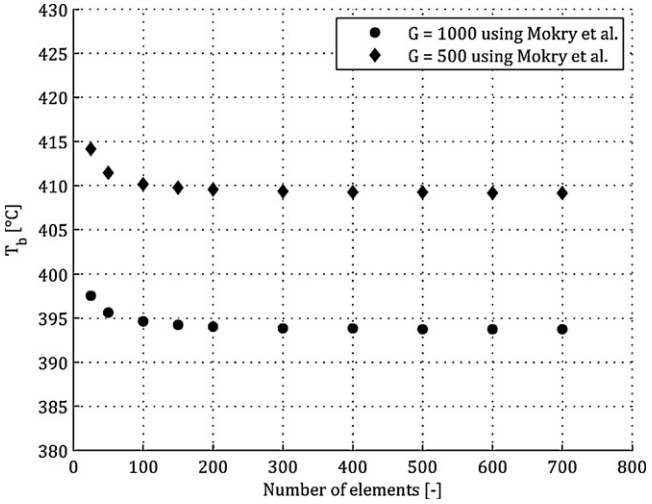

Fig. 11. Mesh convergence analysis for the 1D model using the Nusselt correlation of Mokry et al. [8].

2. 1D heat transfer model of a flow reactor with supercritical water

The governing equations described in Section 1.3 can be simplified by using a 1D modeling approach in order to develop a fast simulation tool with reasonable accuracy. With this aim in mind, the tube is described using a plug flow reactor model [23]. By disregarding all variations in radial direction, the dimensions of computational domain are reduced to only one coordinate. Moreover, all terms having no major contribution to the solution are neglected, which results in a set of equations that can be solved efficiently.

This section contains a detailed description of the simplification procedure. In addition, three Nusselt correlations are selected from literature to close the set of simplified equations. The accuracy of the new model is assessed in Section 3 by comparing the calculation results to experimental data found in Mokry et al. [8].

2.1. Physical and computational domain

Due to the plug flow assumption only variations in axial direction are considered, so that the radial coordinate is of no importance in the calculations. However, there still needs to be a temperature difference across the radius in order to describe heat transfer through the tube wall. Since it is impossible to physically describe the heated tube flow using only one spatial dimension, a distinction is made between the physical and computational domain to give more insight into the modeling approach. The physical domain is represented by a 2D fluid domain that is bounded by an infinitely thin tube wall as shown in Fig. 9.

The schematic temperature and velocity profiles $T'(r,z)$ and $u'(r,z)$ shown in the figure become averaged quantities $T(z)$ and $u(z)$ in the computational domain. Since the model equations will be independent of the radial coordinate, the physical domain can be reduced to a line in the computational domain (Fig. 10).

On basis of a mesh convergence analysis using the bulk temperature as the indicative variable, the domain has been divided into 750 elements for the simulations. The results of the convergence analysis using the conditions of Cases 1 and 2, defined in Table 1, are plotted in Fig. 11, showing an estimated accuracy of within 1 K for this mesh. The chosen mesh size leads to CPU-times of a couple of seconds on a single-core laptop for a tube length of 4.0 m.

In the one-dimensional computational domain, the heat source term $\dot{Q}$ in Eq. 13 can be used to account for the heat that is transferred from the tube wall to the fluid by convection [24]. The heat addition per unit time in an infinitesimal control volume dV is:

$$\dot{Q}dV = -(\vec{q}\cdot\vec{n}_w)dS_w \tag{13}$$

where $\vec{n}_w$ is the outward-pointing normal unit vector on the wall of the fluid domain and dS_w the surface area of the outer tube wall surrounding the control volume. The convective heat flux is modeled by Newton's law of cooling:

$$-\vec{q}\cdot\vec{n}_w \equiv q_w = h(T_w - T) \tag{14}$$

where the heat transfer coefficient h follows from a Nusselt correlation found in the literature. A discussion of available Nusselt correlations for supercritical water flows is found in Section 2.3. Combining Eqs. (13) and (14) gives:

$$\dot{Q} = \frac{4}{D}h(T_w - T) \tag{15}$$

2.2. 1D model equations

This section describes the steps taken to derive the 1D model equations from the governing equations given in Section 1.1. The simplification starts by writing the equations in one-dimensional form and by assuming a system operating in steady state. The mass conservation equation, Eq. (1), then becomes:

$$\frac{d}{dz}(\rho u) = 0 \tag{16}$$

Eq. (16) shows that the mass flux ρu is constant. Although this quantity is exactly equal to G, defined in Section 1.3, the mass flux will be written as $(\rho u)_0$ in the conservation equations for clarity.

In the momentum equation, Eq. (2), the z-component of the volumetric force vector is equal to the gravitational acceleration:

$$f_z = -g \tag{17}$$

The dilatational viscosity κ in Eq. (3) is usually neglected for practical purposes because the availability of these data is very limited. It is besides important only when considering effects where fluid compressibility is essential, such as shock waves and sound propagation, and can therefore be omitted in this study as well. The divergence of the viscous stress tensor for a one-dimensional plug flow then reduces to:

$$\vec{\nabla}\cdot\vec{\vec{\tau}} = -\frac{4}{3}\mu\frac{d^2u}{dz^2} \tag{18}$$

where μ is the dynamic viscosity of the fluid. After substitution of Eqs. (17) and (18) and subtraction of Eq. (16), the equation for momentum conservation given by Eq. (2) becomes:

$$\rho u\frac{du}{dz} = -\frac{dp}{dz} + \frac{4}{3}\mu\frac{d^2u}{dz^2} - \rho g \tag{19}$$

When the kinetic energy in the fluid is assumed to be negligible in comparison with the internal energy, a simplified form of the energy equation can be used in which the temperature appears [1]. This equation can be derived from the total energy equation by assuming that the mechanical energy is negligible. The procedure starts by writing the energy equation in terms of internal energy. The internal energy is by definition related to the total energy by:

$$E \equiv e + \frac{1}{2}|\vec{u}|^2 \tag{20}$$

Substitution of Eq. (20) into Eq. 4 results in:

$$\frac{\partial(\rho e + (1/2)\rho|\vec{u}|^2)}{\partial t} = -\vec{\nabla}\cdot\left(\left(\frac{1}{2}\rho|\vec{u}|^2 + \rho e\right)\vec{u}\right) + \rho(\vec{f}\cdot\vec{u}) - \vec{\nabla}\cdot(p\vec{u}) - \vec{\nabla}\cdot(\vec{\vec{\tau}}\cdot\vec{u}) + \dot{Q} - \vec{\nabla}\cdot\vec{q} \tag{21}$$

An expression for the mechanical energy is obtained by taking the dot product of $\vec{u}$ with the momentum equation. Multiplication of Eq. 2 by $\vec{u}$ yields:

$$\frac{\partial}{\partial t}\left(\frac{1}{2}\rho|\vec{u}|^2\right) = -\vec{\nabla}\cdot\left(\frac{1}{2}\rho|\vec{u}|^2\vec{u}\right) + \rho(\vec{f}\cdot\vec{u}) - \vec{\nabla}\cdot(p\vec{u}) - p(-\vec{\nabla}\cdot\vec{u}) - \vec{\nabla}\cdot(\vec{\vec{\tau}}\cdot\vec{u}) - (-\vec{\vec{\tau}}:\vec{\nabla}\vec{u}) \tag{22}$$

Subtracting Eq. (22) from Eq. (21) yields the equation of change for internal energy:

$$\frac{\partial}{\partial t}(\rho e) = -\vec{\nabla}\cdot(\rho e\vec{u}) - p(\vec{\nabla}\cdot\vec{u}) - (\vec{\vec{\tau}}:\vec{\nabla}\vec{u}) + \dot{Q} - \vec{\nabla}\cdot\vec{q} \tag{23}$$

Eq. (23) can be written somewhat more compactly by using the material derivative and the definition of enthalpy $h \equiv e + (p/\rho)$:

$$\rho\frac{Dh}{Dt} = \frac{Dp}{Dt} - \left(\vec{\vec{\tau}}:\vec{\nabla}\vec{u}\right) + \dot{Q} - \vec{\nabla}\cdot\vec{q} \tag{24}$$

The term on the left-hand side is evaluated in order to obtain an equation in terms of temperature:

$$\begin{aligned}\rho\frac{Dh}{Dt} &= \rho\left(\frac{\partial h}{\partial T}\right)_p\frac{DT}{Dt} + \left(\frac{\partial h}{\partial p}\right)_T\frac{Dp}{Dt}\\ &= \rho C_p\frac{DT}{Dt} + \rho\left[\frac{1}{\rho} - T\left(\frac{\partial(1/\rho)}{\partial T}\right)_p\right]\frac{Dp}{Dt}\\ &= \rho C_p\frac{DT}{Dt} + \left[1 + \frac{T}{\rho}\left(\frac{\partial\rho}{\partial T}\right)_p\right]\frac{Dp}{Dt}\end{aligned} \tag{25}$$

Substitution into Eq. (24) gives the equation of change for temperature:

$$\rho C_p\frac{DT}{Dt} = -\frac{T}{\rho}\left(\frac{\partial\rho}{\partial T}\right)_p\frac{Dp}{Dt} - (\vec{\vec{\tau}}:\vec{\nabla}\vec{u}) + \dot{Q} - \vec{\nabla}\cdot\vec{q} \tag{26}$$

The local heat flux $\vec{q}$ is described by Fourier's law of heat conduction (Eq. (5)). The second term on the right-hand side of Eq. (26) describes viscous dissipation heating. This quantity is always positive and, for Newtonian fluids, can be written in the form of a viscous dissipation function ϕ_v:

$$-(\vec{\vec{\tau}}:\vec{\nabla}\vec{u}) = \mu\phi_v \tag{27}$$

Substitution of Eqs. (5) and (27) into Eq. (26) and replacing the heat source term by Eq. (15) yields:

$$\rho C_p\frac{DT}{Dt} = -\frac{T}{\rho}\left(\frac{\partial\rho}{\partial T}\right)_p\frac{Dp}{Dt} + \mu\phi_v + \frac{4}{D}h(T_w - T) + \vec{\nabla}\cdot(k\vec{\nabla}T) \tag{28}$$

For one-dimensional flow in steady state this becomes:

$$\rho C_p u\frac{dT}{dz} = -\frac{T}{\rho}\left(\frac{\partial\rho}{\partial T}\right)_p u\frac{dp}{dz} + \frac{4}{3}\mu\left(\frac{du}{dz}\right)^2 + \frac{4}{D}h(T_w - T) + \frac{d}{dz}\left(k\frac{dT}{dz}\right) \tag{29}$$

The momentum and energy Eqs. (19) and (29) can be simplified further by neglecting all terms that have a negligible influence on the exact solution. These terms may be identified if the equations are rewritten in dimensionless form [1]. Evaluation of the resulting dimensionless groups and comparing their order of magnitude provides information on the relative importance of the different terms.

In the following procedure, fluid properties are assumed constant. Density, conductivity and viscosity are taken as the linear average of the minimum and maximum values that are to be expected in the system, which are listed in Table 2.

Table 2
System range for several quantities.

Parameter	Symbol	Unit	Minimum	Maximum
Longitudinal coordinate	z	m	0	4.0
Temperature	T	°C	350	500
Density	ρ	kg/m^3	85	620
Isobaric heat capacity	C_p	kJ/kg K	3	103
Thermal conductivity	k	W/m K	0.1	0.4
Dynamic viscosity	μ	kg/m s	3×10^{-5}	8×10^{-5}

The extrema shown are derived from the properties of water in the range between the inlet temperature and wall temperature. The mean velocity can be derived from Eq. (16) using the mean density. A representative mean value for the heat capacity at isobaric conditions is given by:

$$\overline{C}_p = \frac{1}{T_w - T_{in}}\int_{T_{in}}^{T_w} C_p dT = \frac{h_w - h_{in}}{T_w - T_{in}} \tag{30}$$

where h_w and h_{in} are the specific enthalpy of the fluid at wall and inlet temperature. The dimensionless variables used for the scaling procedure are:

$$\breve{z} = \frac{z}{l} \quad \breve{u} = \frac{u}{\overline{u}} \quad \breve{T} = \frac{T - T_{in}}{T_w - T_{in}} \quad \breve{\rho} = \frac{p - p_0}{\overline{\rho}gl} \tag{31}$$

where l is the length of the heated section of the tube and a bar denotes a system-averaged quantity. Estimations for the contribution of gravity, flow velocity or viscosity on the relative pressure in the system clearly point out that the hydrostatic pressure will be dominant. For this reason, the hydrostatic pressure has been chosen for scaling the relative pressure.

Substitution of the dimensionless variables defined by Eqs. (31) into (19) and (29) gives:

$$\breve{u}\frac{d\breve{u}}{d\breve{z}} = -\frac{gl}{\overline{u}^2}\frac{d\breve{p}}{d\breve{z}} + \frac{\overline{\mu}}{\overline{\rho}\overline{u}l}\frac{4}{3}\frac{d^2\breve{u}}{d\breve{z}^2} - \frac{gl}{\overline{u}^2} \tag{32}$$

Table 3
Estimations of the dimensionless groups based on mean parameter values.

Group	Case 1	Case 2	Case 3
$\frac{1}{Fr}$	5×10^{0}	2×10^{1}	1×10^{2}
$\frac{1}{Re}$	1×10^{-8}	3×10^{-8}	7×10^{-8}
$\frac{Br}{FrPr}$	3×10^{-5}	3×10^{-5}	3×10^{-5}
$\frac{Br}{Pe}$	7×10^{-14}	4×10^{-14}	1×10^{-14}
$\frac{Nu}{Pe_D}$	6×10^{-1}	5×10^{-1}	6×10^{-1}
$\frac{1}{Pe}$	6×10^{-9}	1×10^{-8}	3×10^{-8}

$$\check{u}\frac{d\check{T}}{d\check{z}} = -\frac{gl}{\overline{C}_p\Delta T}\frac{T}{\rho}\left(\frac{\partial\rho}{\partial T}\right)_p \check{u}\frac{d\check{p}}{d\check{z}} + \frac{\overline{\mu u}}{\overline{\rho}\overline{C}_p\Delta T l}\frac{4}{3}\left(\frac{d\check{u}}{d\check{z}}\right)^2 + \frac{hl}{\overline{\rho}\overline{C}_p\overline{u}D}4(1-\check{T}) + \frac{\overline{k}}{\overline{\rho}\overline{C}_p\overline{u}l}\frac{d^2\check{T}}{d\check{z}^2} \tag{33}$$

where $\Delta T \equiv T_w - T_{in}$. Using a more compact notation for the dimensionless groups:

$$\check{u}\frac{d\check{u}}{d\check{z}} = -\frac{1}{Fr}\frac{d\check{p}}{d\check{z}} + \frac{1}{Re}\frac{4}{3}\frac{d^2\check{u}}{d\check{z}^2} - \frac{1}{Fr} \tag{34}$$

$$\check{u}\frac{d\check{T}}{d\check{z}} = -\frac{Br}{FrPr}\frac{T}{\rho}\left(\frac{\partial\rho}{\partial T}\right)_p \check{u}\frac{d\check{p}}{d\check{z}} + \frac{Br}{Pe}\frac{4}{3}\left(\frac{d\check{u}}{d\check{z}}\right)^2 + \frac{Nu}{Pe_D}4(1-\check{T}) + \frac{1}{Pe}\frac{d^2\check{T}}{d\check{z}^2} \tag{35}$$

Since the dimensionless quantities are now scaled to values between 0 and $\mathcal{O}(10)$, the values of the dimensionless groups indicate which terms are negligible. For the three cases considered in this study, the following values have been calculated using the average of the parameter values listed in Table 2.

Here the heat transfer coefficient in the Nusselt number is assumed to be 15,000 W/m^2 K in case 1, 6000 W/m^2 K in case 2 and 3000 W/m^2 K in case 3. These values are representative according to measurement data found in Mokry et al. [8] for a tube diameter of 10 mm. Based on the estimations presented in Table 3, it can be concluded that viscous effects, internal conduction and enthalpy changes due to a pressure gradient may be neglected without losing much accuracy compared to the full 1D model equations. This results in:

$$\frac{d}{dz}(\rho u) = 0 \tag{36}$$

$$(\rho u)_0\frac{du}{dz} + \frac{dp}{dz} = -\rho g \tag{37}$$

$$\frac{dT}{dz} = \frac{4}{D}\frac{h}{(\rho u)_0 C_p}(T_w - T) \tag{38}$$

where the second fraction on the right-hand side of Eq. (38) is also known as the Stanton number:

$$St = \frac{h}{\rho u C_p} \tag{39}$$

For numerical implementation, it is convenient to write this system of equations into the form:

$$A(\vec{y},z)\frac{d\vec{y}}{dz} = \vec{F}(\vec{y},z) \tag{40}$$

where $\vec{y}$ is the vector of flow variables, $A(\vec{y},z)$ is a characteristic matrix and $F(\vec{y},z)$ is a vector of source terms. When p, u and T are chosen as the flow variables, the model equations are represented by:

$$\begin{bmatrix} 0 & \frac{1}{u} & 0 \\ 1 & (\rho u)_0 & 0 \\ 0 & 0 & 1 \end{bmatrix}\frac{d}{dz}\begin{Bmatrix} p \\ u \\ T \end{Bmatrix} = \begin{Bmatrix} -\frac{1}{\rho}\frac{d\rho}{dz} \\ -\rho g \\ \frac{4}{D}\mathrm{St}(T_w - T) \end{Bmatrix} \tag{41}$$

Dividing by matrix A yields:

$$\frac{d}{dz}\begin{Bmatrix} p \\ u \\ T \end{Bmatrix} = \begin{bmatrix} -u(\rho u)_0 & 1 & 0 \\ u & 0 & 0 \\ 0 & 0 & 1 \end{bmatrix}\begin{Bmatrix} -\frac{1}{\rho}\frac{d\rho}{dz} \\ -\rho g \\ \frac{4}{D}\mathrm{St}(T_w - T) \end{Bmatrix} \tag{42}$$

This system of equations has been solved explicitly for the pressure, axial velocity and temperature using an Euler scheme.

2.3. Nusselt correlations

Quite a number of Nusselt correlations have been developed for supercritical heat transfer in tube flows. Most of these empirical correlations have the general form of a modified Dittus–Boelter equation [25]:

$$Nu_x = C\cdot \mathrm{Re}_x^n \cdot \mathrm{Pr}_x^m \cdot F_c \tag{43}$$

where x is an indicator for the temperature which is used to calculate the fluid properties, C is a constant and F_c is a correction factor that accounts for property variations or entrance effects. A selection of Nusselt correlations found in literature that may be suitable for predicting the heat transfer coefficient in this study is given in Table 4. A mathematical description of the correlations in the form of Eq. (43) is found in Table 5.

The correlation of Swenson et al. [26] has been derived from experimental data of upward supercritical water flows. It evaluates the majority of fluid properties at wall temperature. Yamagata et al. [18] conducted experiments on horizontal and vertical supercritical water flows. The most extensive data were obtained for the vertically upward flow in a 10 mm tube. After excluding the measurements obtained in the region of deteriorated heat transfer, mainly these data were used to derive the proposed correlation. The correlation includes a correction factor depending on the Eckert number E, which is defined as:

$$E = \frac{T_{pc} - T_b}{T_w - T_b} \tag{44}$$

Mokry et al. [8] derived a correlation on basis of measurements conducted at the supercritical test facility of the Institute for Physics and Power Engineering in Obninsk, Russia. The experimental data were collected from supercritical water flows in 10 mm pipes.

2.4. Boundary conditions

The 1D heat transfer model requires inlet conditions to calculate further towards the end of the tube. In addition, the wall temperature is needed as a boundary condition. The inlet and boundary conditions are set as listed in Table 1. These conditions are in agreement with the conditions that were selected for measurements in supercritical water found in Mokry et al. [8], which enables validation of the simulation results. The experimental data includes measurements of the inner wall temperature for a heated upflow of water using uniform wall heat flux. The inner wall temperature data has been adopted as the wall condition for the simulations.

On basis of the validity ranges shown in Table 4, the Nusselt correlations of Swenson et al., Yamagata et al. and Mokry et al. have been selected to prescribe the local heat transfer from the wall

Table 4
A selection of Nusselt correlations for heated, aiding tube flow at supercritical pressures and their parameter ranges.

Correlation	p [MPa]	G [kg/m^2 s]	Q [kW/m^2]	D [mm]	T_b [°C]
Swenson et al. [26]	23–41	542–2150	200–2000	9.4	75–576
Yamagata et al. [18]	23–29	310–1830	120–930	7.5, 10	230–540
Mokry et al. [8]	24	200–1500	$\leq$ 1250	10	320–406

Table 5
Description of the selected Nusselt correlations according to Eq. (43).

Correlation	x	C	n	m	F_c
Swenson et al. [26]	w	0.00459	0.923	0.613	$\left(\frac{\bar{C}_p}{C_{p,w}}\right)^{0.613}\left(\frac{\rho_w}{\rho_b}\right)^{0.231}$
Yamagata et al. [18]	b	0.0135	0.85	0.8	$F=\begin{cases}1.0 & \text{for } E>1\\ 0.67\cdot Pr_{pc}^{-0.05}\left(\frac{\bar{C}_p}{C_{p,b}}\right)^{n_1} & \text{for } 0\leq E\leq 1\\ \left(\frac{\bar{C}_p}{C_{p,b}}\right)^{n_2} & \text{for } E<0\end{cases}$
Mokry et al. [8]	b	0.0061	0.904	0.684	$\left(\frac{\bar{C}_p}{C_{p,b}}\right)^{0.684}\left(\frac{\rho_w}{\rho_b}\right)^{0.564}$

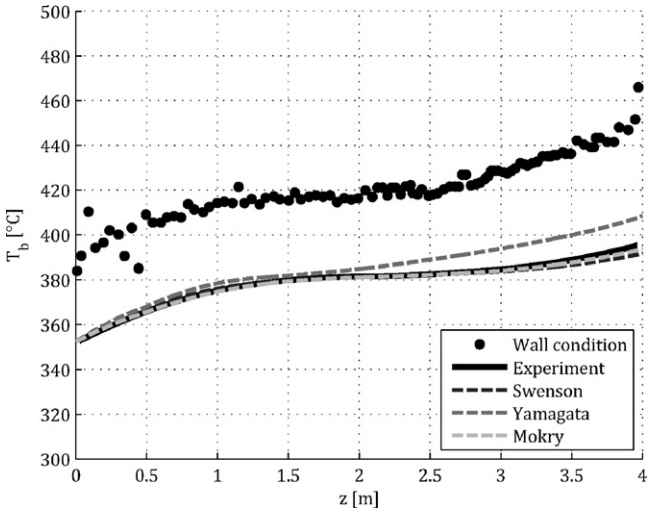

Fig. 12. Temperature as function of the tube height for $G = 1000$ kg/m^2 s using different Nusselt correlations. Experimental data reproduced with permission of Elsevier.

to the fluid. These three correlations result in three temperature profiles for each of the considered mass fluxes.

Since the density gradient in the elements, $d\rho/dz$ in Eq. (42), is calculated using backward differences, this gradient is assumed to be zero for the first element to avoid numerical errors.

3. Results and validation

The 1D heat transfer model presented in this article has been used to predict the bulk-fluid temperature for the cases shown in Table 1. Temperature predictions using the correlations of Swenson et al., Yamagata et al. and Mokry et al. have been compared to experimental data found in Mokry et al. [8]. The experimental temperature profiles were constructed by measuring the bulk-fluid temperature at the inlet and outlet and then calculating the profiles using a simple heat balance (I.L. Pioro, personal communication, December 14, 2011).

The calculated fluid temperature profiles for a mass flux of 1000 kg/m^2 s are shown in Fig. 12 together with the experimental data. This case fits well within the ranges of validity listed in Table 4. The slope of the temperature profile decreases while approaching the pseudo-critical point at 381 °C. The phase change requires a lot of energy due to the high heat capacity in the vicinity of this point, causing the temperature increase to slow down. Once the fluid temperature has passed the pseudo-critical point, the slope of the lines tends to restore. When the bulk temperature is raised further, the rate of heat transfer is expected to decline since the driving force will decrease. The decrease is not visible in the results, however, which indicates that the heat transfer may still be governed by other effects like for example boiling effects.

The best match with the measurements is obtained when using the correlation of Mokry et al. or Swenson et al. The excellent agreement in temperature profiles demonstrates that, in case a suitable Nusselt correlation is available, the model is capable of accurately calculating the fluid temperature from wall temperature data at supercritical conditions. The correlation of Yamagata results in a good match up to the region where the fluid reaches pseudocritical conditions. From this point, the rate of heat transfer and hence temperature is overpredicted. Apparently, the large hump in the heat flux around the the pseudocritical point seen in Fig. 13 is not realistic for this case.

The graphs illustrate that not all correlations give similar results, despite of the fact that they should all be applicable for this case. Therefore, selecting the right correlation solely based on the parameters considered in Table 4 may not be adequate. In order to study the sensitivity of the selected Nusselt correlations to the mass flux, a second and third case have been simulated using a mass flux of 500 and 200 kg/m^2 s, respectively. The results are shown in Fig. 14 and 15, together with the experimental data for this particular mass flux.

Figs. 14 and 15 show that the correlations of Mokry et al. and Swenson et al. give accurate predictions of the bulk temperature for these mass fluxes as well. The results based on the correlation of Yamagata et al. are however worse compared to the results in Fig. 12.

Fig. 16 points out that the heat flux for $G = 200$ kg/m^2 s is again overpredicted in a broad range around the pseudocritical temperature. The heat flux graphs for $G = 500$ kg/m^2 s are similar, but have been omitted here to save space. Clearly, the correlation of Yamagata et al. is outperformed by the correlation of Swenson et al., even though the validity range of the latter does not include these low mass fluxes.

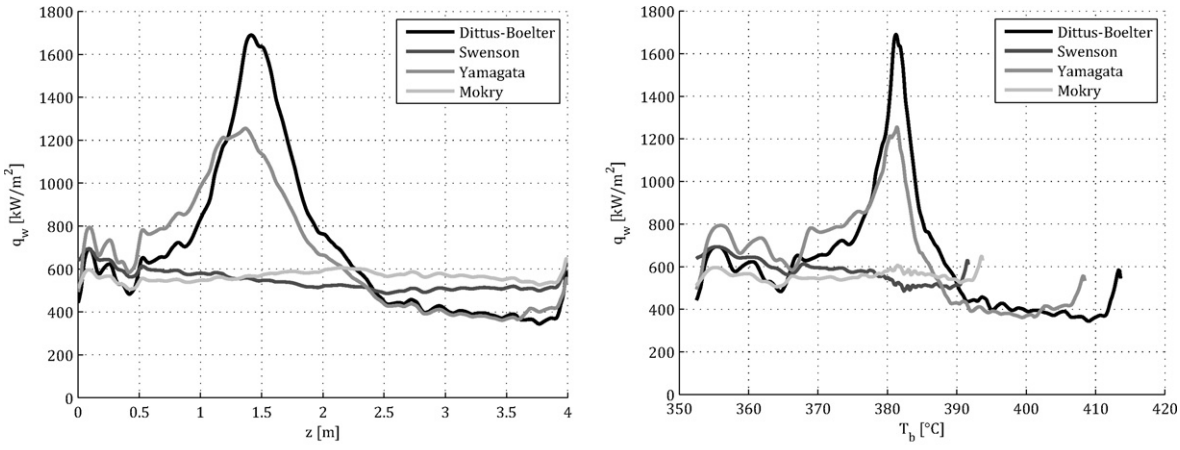

(a) Heat flux as function of tube height. (b) Heat flux as function of bulk temperature.

Fig. 13. Wall heat flux as function of the tube height (a) and bulk temperature (b) for $G = 1000\ \mathrm{kg/m^2\ s}$ using different Nusselt correlations.

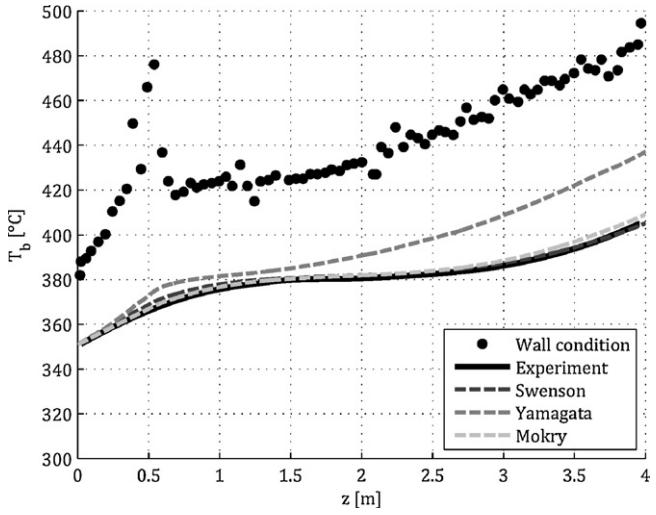

Fig. 14. Temperature as function of the tube height for $G = 500\ \mathrm{kg/m^2\ s}$ using different Nusselt correlations. Experimental data reproduced with permission of Elsevier.

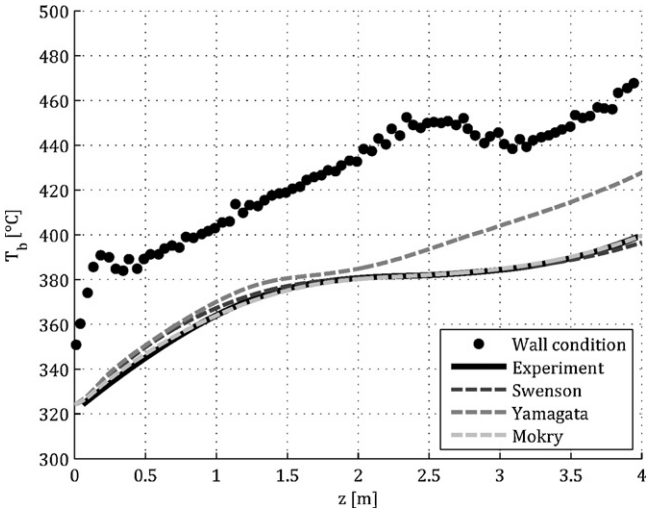

Fig. 15. Temperature as function of the tube height for $G = 200\ \mathrm{kg/m^2\ s}$ using different Nusselt correlations. Experimental data reproduced with permission of Elsevier.

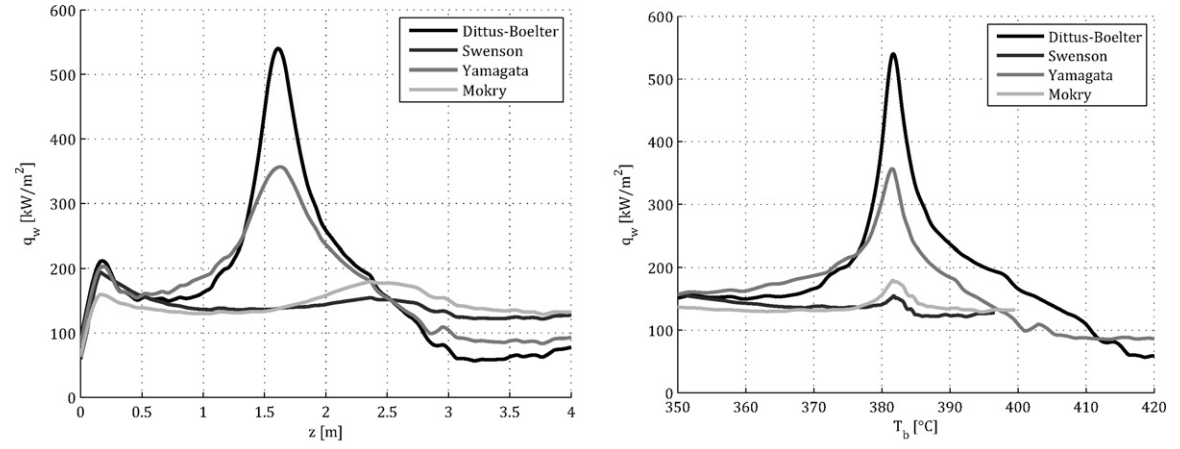

(a) Heat flux as function of tube height. (b) Heat flux as function of bulk temperature.

Fig. 16. Wall heat flux as function of the tube height (a) and bulk temperature (b) for $G = 200\ \mathrm{kg/m^2\ s}$ using different Nusselt correlations.

4. Discussion

The large deviation between results based on the correlation of Yamagata et al. and results based on the other two correlations may be explained by considering boiling effects. According to the theory of heat transfer at supercritical pressures (Section 1), pseudo-film boiling can highly influence heat transfer at supercritical pressures depending on the flow conditions. A combination of several parameters including tube diameter, pressure, mass flux and heat flux determines which heat transfer regimes will occur inside the tube (i.e. normal, improved or deteriorated heat transfer).

For the cases considered in this study, the heat flux seems to exceed or approach the critical value indicated by Fig. 4. Therefore, it can be expected that peaks in the heat flux around the pseudo-critical point are lower, flattened or do not occur at all. In contrast to the other two correlations considered in this study, the correlation of Yamagata et al. was derived from experimental data from which measurements obtained in the region of deteriorated heat transfer were excluded [18]. This is a possible reason why the heat flux predicted by Yamagata et al. is incorrect for the cases considered in this article. In cases where deterioration of heat transfer does not occur, the correlation might show better accuracy.

The influence of buoyancy forces can be estimated by calculating the criterion of Aicher and Martin (Eq. (9)). In Case 3, the value of this criterion mainly varies between 0.05 and 0.2 over the first half of the tube. According to Fig. 5, the flow in this region should hence be classified as aided mixed convective flow, for which the Nusselt number is significantly lower compared to pure forced convection. Here, both buoyancy forces and pseudo-film boiling could have been responsible for the low heat transfer rates. However, heat transfer rates in Case 1 are also much lower than predicted by the Dittus–Boelter equation, whereas this case should be classified as (nearly) pure forced convection over the entire tube length. With values lower than 0.08 for the criterion, buoyancy forces are probably not the cause for the low heat transfer rates in this case. In Case 2, only a small region of mixed convective flow is observed near the inlet, which cannot explain the decreased heat transfer rate over a large part of the tube.

Assuming that boiling effects are the main reason for the large differences between the predictions observed in Section 3, it is important to know on beforehand if the critical heat flux will be exceeded when selecting a Nusselt correlation for the 1D model. An estimation for the critical heat flux can be made using the criteria proposed by Yamagata et al., Eq. (7), or by Mokry et al., Eq. (8). However, it should be noted that there is still no unique definition for the onset of heat transfer deterioration, because this phenomenon behaves rather smoothly [9].

The sensitivity of the results for other parameters than mass flux has not been studied by the authors. In order to study the influence of boiling effects for this tube geometry in more detail, a two-dimensional model has been developed and will be presented in a next article.

5. Conclusions

Based on a literature study, it can be concluded that the property variations of water in the vicinity the (pseudo)critical point significantly influence the heat transfer. Depending on the flow conditions, the variations in fluid properties can result in heat transfer enhancement or deterioration. In literature, these effects have been related to boiling phenomena and to acceleration of the fluid due to buoyancy forces. Acceleration of the fluid near the boundary layer is assumed to influence the turbulent diffusivity in the region where turbulence plays an important role in the heat transfer.

In this work, heat transfer to supercritical water has been modeled in a one-dimensional domain by using a plug flow approach. Viscous effects, internal conduction and enthalpy changes due to a pressure gradient have been neglected after evaluation of the governing equations in dimensionless form. Nusselt correlations are required for predicting the heat transfer coefficient in order to close the set of equations.

The results of the simulations for three different cases show that the model is able to accurately predict the bulk temperature based on heat transfer rates provided by a suitable Nusselt correlation. However, the results also give reason to assume that the correlations are very specific for the flow conditions of the experiments from which the Nusselt correlations were derived. Different correlations that are all valid for the selected operating conditions do not necessarily give the same result.

The large deviation between the predictive capability of the correlations suggest that it is important to consider boiling effects that occur when a critical heat flux is reached. Although the agreement with a 2D simulation is yet to be investigated in a subsequent article, it can be said that the accuracy of the correlation for the simulated case will be crucial for the quality of the 1D model.

References

[1] R. Bird, W. Stewart, E. Lightfoot, Transport Phenomena, John Wiley & Sons, New York, 1960.
[2] R. Kee, M. Coltrin, P. Glarborg, Chemically Reacting Flow: Theory and Practice, LibreDigital, 2003.
[3] W. Wagner, J. Cooper, A. Dittmann, J. Kijima, H. Kretzschmar, A. Kruse, R. Mareš, K. Oguchi, H. Sato, I. Stöcker, et al., The IAPWS industrial formulation 1997 for the thermodynamic properties of water and steam, Journal of Engineering for Gas Turbines and Power 122 (2000) 150.
[4] W. Wagner, A. Pruss, The IAPWS Formulation 1995 for the thermodynamic properties of ordinary water substance for general and scientific use, Journal of Physical and Chemical Reference Data 31 (2) (1999) 387.
[5] W. Wagner, H. Kretzschmar, International Steam Tables: Properties of Water and Steam based on the Industrial Formulation IAPWS-IF97: Tables, Algorithms, Diagrams, and CD-ROM Electronic Steam Tables: All of the Equations of IAPWS-IF97 Including a Complete Set of Supplementary Backward Equations for Fast Calculations of Heat Cycles, Boilers, and Steam Turbines, Springer Verlag, 2008.
[6] R. Fernández-Prini, R. Dooley, Revised release on the IAPWS formulation 1985 for the thermal conductivity of ordinary water substance, The International Association for the Properties of Water and Steam (1998).
[7] K. Watanabe, R. Dooley, Revised release on the IAPWS formulation 1985 for the viscosity of ordinary water substance, The International Association for the Properties of Water and Steam (2003).
[8] S. Mokry, I. Pioro, A. Farah, K. King, S. Gupta, W. Peiman, P. Kirillov, Development of supercritical water heat-transfer correlation for vertical bare tubes, Nuclear Engineering and Design 241 (4) (2011) 1126–1136.
[9] X. Cheng, T. Schulenberg, Heat Transfer at Supercritical Pressures: Literature Review and Application to an HPLWR, FZKA, 2001.
[10] F. Dittus, L. Boelter, Heat transfer in automobile radiators of the tubular type, International Communications in Heat and Mass Transfer 12 (1) (1985) 3–22.
[11] A. Belmiloudi, Heat Transfer – Theoretical Analysis, Experimental Investigations and Industrial Systems, 1st, Intech, 2011.
[12] R. Sinnott, MyiLibrary, Coulson & Richardson's Chemical Engineering [Electronic Resource]: Chemical Engineering Design, Butterworth-Heinemann, 2005.
[13] V. Dhir, Boiling heat transfer, Annual review of fluid mechanics 30 (1) (1998) 365–401.
[14] X. Cheng, B. Kuang, Y. Yang, Numerical analysis of heat transfer in supercritical water cooled flow channels, Nuclear Engineering and Design 237 (3) (2007) 240–252.
[15] J. Jackson, W. Hall, Forced convection heat transfer to fluids at supercritical pressure, Turbulent Forced Convection in Channels and Bundles 2 (1979) 563–612.
[16] H. Ogata, S. Sato, Measurements of forced convection heat transfer to supercritical helium, in: Fourth International Cryogenic Engineering Conference, Eindhoven, the Netherlands, 1972.
[17] B. Petukhov, V. Kurganov, V. Ankudinov, Heat transfer and flow resistance in the turbulent pipe flow of a fluid with near-critical state parameters, Teplofizika Vysokikh Temperatur 21 (1983) 92–100.
[18] K. Yamagata, K. Nishikawa, S. Hasegawa, T. Fujii, S. Yoshida, Forced convective heat transfer to supercritical water flowing in tubes, International Journal of Heat and Mass Transfer 15 (12) (1972) 2575–2593.
[19] J. Licht, M. Anderson, M. Corradini, Heat transfer to water at supercritical pressures in a circular and square annular flow geometry, International Journal of Heat and Fluid Flow 29 (1) (2008) 156–166.

[20] T. Aicher, H. Martin, New correlations for mixed turbulent natural and forced convection heat transfer in vertical tubes, International Journal of Heat and Mass Transfer 40 (15) (1997) 3617–3626.
[21] G. Celata, F. D'Annibale, A. Chiaradia, M. Cumo, Upflow turbulent mixed convection heat transfer in vertical pipes, International Journal of Heat and Mass Transfer 41 (24) (1998) 4037–4054.
[22] H. Tanaka, S. Hatano, S. Maruyama, Combined forced and natural convection heat transfer for upward flow in a uniformly heated vertical pipe: series b: fluids engineering, heat transfer, combustion, power, thermophysical properties, JSME International Journal: Bulletin of the JSME 30 (266) (1987) 1348.
[23] P. Atkins, J. De Paula, Atkins' physical chemistry, Chemistry (2006).
[24] F. Incropera, D. De Witt, Fundamentals of Heat and Mass Transfer, John Wiley and Sons Inc., New York, NY, 1985.
[25] J. Yu, B. Jia, D. Wu, D. Wang, Optimization of heat transfer coefficient correlation at supercritical pressure using genetic algorithms, Heat and Mass Transfer 45 (6) (2009) 757–766.
[26] H. Swenson, J. Carver, C. Kakarala, Heat transfer to supercritical water in smooth-bore tubes, Journal of Heat Transfer, Transaction ASME, Series C 87 (4) (1965) 477–484.